ISSN 0023-1584, Kinetics and Catalysis, 2012, Vol. 53, No. 2, pp. 197–205. © Pleiades Publishing, Ltd., 2012.

Photocatalytic Activity of Au/TiO_2 Nanocomposite for Azo-Dyes Degradation[1]

Nruparaj Sahu and K. M. Parida

Colloids and Materials Chemistry Department, Institute of Minerals and Materials Technology (CSIR), Bhubaneswar, Orissa, India

e-mail: paridakulamani@yahoo.com

Received October 10, 2010

Abstract—The structural properties of Au/TiO_2 catalyst were studied by X-ray diffraction, UV-visible diffuse reflectance, photoluminescene, scanning transmission and electron microscope, and temperature programmed reduction. The photocatalytic activity of the catalysts was evaluated for the degradation of various azo-dyes such as methylene blue, methyl orange, reactive blue-4, and eosin-B under solar irradiation. It was found that TiO_2 catalyst modified with gold exhibits higher percentage of degradation compared to starting TiO_2. For example, TiO_2 showed 35% of methyl orange degradation whereas gold modified TiO_2 possessed 82%. Effect of different parameters such as pH and dye concentration has been evaluated and the photocatalytic activity was correlated with physico-chemical properties. The dye degradation rate followed first order kinetics.

DOI: 10.1134/S0023158412020097

Heterogeneous photocatalysis is an attractive method for the degradation of various organic pollutants [1–3]. Among the various metal oxide semiconductor materials, TiO_2 is probably the most widely studied material because of its low-cost, nontoxic, strong oxidizing power, long-term stability against photocorrosion and strong metal–support interaction [4–6]. A good photocatalyst depends strongly on its optical absorption properties and efficiency in electron–hole pair separation. The large band gap (3.2 eV) of anatase titania restricts its photocatalytic applications to the UV range (less than 387 nm). This practically rules out the use of sunlight as an energy source as it contains 3–4% of UV and 43% of visible light. Many attempts have been made to modify TiO_2 by metal doping so as to shift the absorbance maxima to visible light, to eliminate the electrons/holes recombination and to increase the quantum efficiency [7, 8]. Highly crystalline materials can be synthesized by metal ion doping, which facilitate the electron transfer from TiO_2 to metal nanoparticles. This process decreases electron/hole recombination events and thus increases the photocatalytic efficiency. Choi et al. carried out a systematic study on the enhanced effect of 21 different transitional metal ions on the photocatalytic activity of quantum-sized TiO_2 in both chloroform oxidation and carbon tetrachloride reduction [9]. Recently, Zhang et al. reported that TiO_2–montmorillonite composite exhibits excellent photocatalytic activity for methylene blue degradation [10]. They also reported photocatalytic degradation of methyl orange under visible light over CuO_2 [11]. Shie et al. reported the photocatalytic activity of Fe and Ho co-doped TiO_2 for photocatalytic degradation of methyl orange in an aqueous suspension under UV and simulated solar light illumination [12].

Gold dispersed as ultra fine particles and supported on metal oxides exhibits extraordinary catalytic activity for various reactions including CO oxidation, water-gas shift reaction, low temperature catalytic combustion, and photocatalysis [13–18]. Arabatzis et al. studied the photocatalytic activity of Au/TiO_2 for methyl orange degradation and found that gold deposition improves the photocatalytic efficiency of the titania films by the synergetic action on the charge separation process onto the semiconductor [19]. A increase significant in photocatalytic destruction of oxalic acid over gold modified titania has been reported [20]. Sonawane et al. found that using of Au/TiO_2 thin film increases the photocatalytic activity in phenol degradation more than 2–2.3 times [21]. Li et al. synthesized highly active mesoporous Au/TiO_2 nanocomposites with significantly improved photocatalytic activity. They found that enhanced light absorption and improved quantum efficiency are the main factors for the improved photocatalytic activity [22]. Au/TiO_2 nanocrystals with interparticulate mesopores are highly efficient photocatalysts for the oxidation of methanol [23]. Antenna-like mechanism for the photogenerated electrons diffusion and charge

[1] The article is published in the original.

separation was proposed to explain these unexpected findings. Wang et al. studied number of synthesis routes to fabricate porous Au/TiO_2 nanocomposites using template assisted technique and found enhanced photocatalytic activity under UV light irradiation for photodecomposition of methylene blue [24]. Jung et al. reported a review on photocatalytic activity of the amorphous Au-buffered TiO_2 thin films. Au/TiO_2 thin film was found to be superior to pure anatase TiO_2 thin films because the Au-buffer layers inhibit the electron/holes recombination [25]. Recently Yu et al. reported the enhanced photocatalytic activity of Au/TiO_2 composite microspheres for the decomposition of formaldehyde [26].

The present study deals with the photocatalytic activities of Au/TiO_2 nanocomposites towards degradation of azo-dyes such as methylene blue (**MB**), methyl orange (**MO**), reactive blue-4 (**RB 4**) and eosin-B (**EB**) under solar light radiation. Effect of different parameters such as pH, concentration and reaction kinetics has been reported.

EXPERIMENTAL

Materials Preparation

Hydrated TiO_2 was prepared by sol-gel method, taking titanium isopropoxide as the starting material. In a typical preparation procedure, 50 mL of titanium isopropoxide was dissolved in 400 mL of isopropanol. To this solution, 12.7 mL of distilled water adjusted to pH 3.0 by 1 M HNO_3 was added dropwise under vigorous stirring. The resulting colloidal suspension was stirred for 3 h and aged at 80°C for 10 h. The gel obtained was filtered, washed and dried at 100°C for 12 h. The prepared sample was heated in a muffle furnace at a heating rate of 10°C/min up to 400°C and held at the upper temperature for 4 h.

Gold (1 wt %) promoted TiO_2 (as synthesized) sample was prepared by borohydrate reduction method. The support was suspended in deionized water and required amount of dilute $HAuCl_4$ (0.01 mol/L) was added drop wise with continuous stirring. Two hours after complete addition of the gold precursor, the pH was raised to 8.5 using 15% NH_4OH and aged for a further period of 2 h. The required amount of freshly prepared $NaBH_4$ in deionized, cooled to ice water temperature was rapidly added to the mixture using a syringe to ensure complete reduction of Au(III) to Au(0). The suspension was then filtered, washed several times with warm deionized water and dried overnight at 120°C for 12 h. This sample is denoted as Au/TiO_2.

Characterization

Surface morphologies (i.e., size, shape and arrangement of the particles which make up the specimen) as well as their relationship to each other on the atomic scale were observed through a transmission electronic microscope (**TEM**, FEI, TECNAI G^2 20, TWIN) operating at 200 kV. The samples for electron microscopy were prepared by dispersing the powder in ethanol and coating a very dilute suspension on carbon coated Cu grids. TEM images were recorded by using Gatan CCD camera. The particle sizes were determined by using several TEM micrographs and the IMAGEJ analysis package.

The structure and phase identification were characterized by X-ray diffraction (**XRD**, Philips 1710, CuK_α radiation).

The optical absorbance was recorded in UV-vis spectrometer (Shimadzu).

The diffuse reflectance spectra (**DRS**) were recorded in the range of 200–800 nm using boric acid as the standard.

Fluorescence measurements were carried out with a Hitachi F-4500 spectrofluorimeter, with a 150 W xenon lamp as the light source under photoexcitation at 380 nm.

Temperature programmed reduction (**TPR**) was performed using CHEMBET-3000 (Quantachrome, USA) instrument in the temperature range of 40–800°C. About 0.1 g of powdered sample was taken in quartz U-form tube and degassed at 523 K for 1 h with nitrogen gas, then cooled to room temperature. For TPO, 5% O_2 (balanced with helium) gas was flowed through the sample maintaining a heating rate of 10°C/min to record the profile. For TPR, 10% H_2 gas was flowed through the sample maintaining a heating rate of 10°C/min to record the profile.

X-ray photoelectron spectra (**XPS**) were recorded on a VG Microtech Multilab ESC A 3000 spectrometer that was equipped with an AlK_α X-ray source ($h\nu$ = 1486.6 eV). Binding energy calibration was performed with C1*s* core level at 284.6 eV.

Fourier transform infra-red (**FT-IR**) spectra of the samples were recorded in a Varian FTIR spectrophotometer (FTS-800) in the range of 400–4000 cm^{-1} taking KBr as the reference.

The point of zero charge (isoelectric point) of Au/TiO_2 particles was measured with a Particle Charge Detector (PCD-03-pH) apparatus (Mutek, Herrching, Germany), the working principle is described elsewhere [27].

In situ FT-IR CO adsorption study was performed in transmission mode on a JASCO 610 FT-IR spectrophotometer. Prior to dosing with CO, the sample wafer was subjected to overnight degassing at 300°C.

Normally, 300 scans were coadded, and the spectra were recorded using a similarly treated but unexposed pellet as background [28].

Photocatalytic Reaction and Dark Adsorption

Taking 20 ml of 100 mg/L of solution in a 100 mL closed Pyrex flask, over 1.0 g/L of catalyst, carried out the photocatalytic degradation of MO, MB, RB-4 and EB. Structural formulae of these dyes are given beneath:

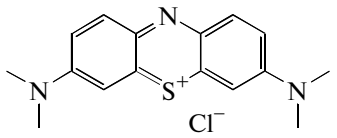

Methylene Blue

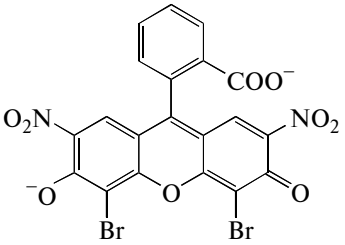

Eosin B

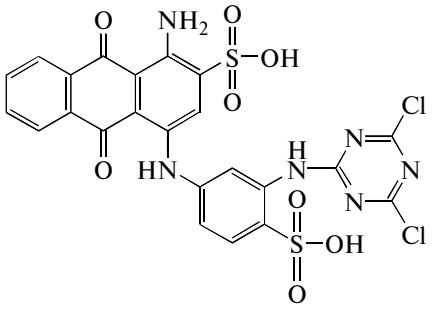

Reactive Blue-4

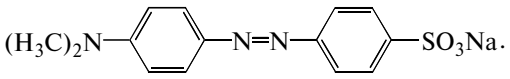

Methyl Orange

All these dyes solution were kept 15 min in dark for adsorption before expose to light for photodegradation. The solutions were exposed to sunlight with constant stirring. All the irradiation was performed in triplicate during March 2007 (sunny days), from 10:00 a.m. to 14:00 p.m. when the average solar intensity was 0.80 kW/m^2 and the intensity fluctuations were minimal. Reactions were performed also in the dark in order to determine the adsorption behaviour of the catalysts under similar conditions. Blank experiment was performed taking dye solution without catalyst to know the extent of degradation due to solar radiation.

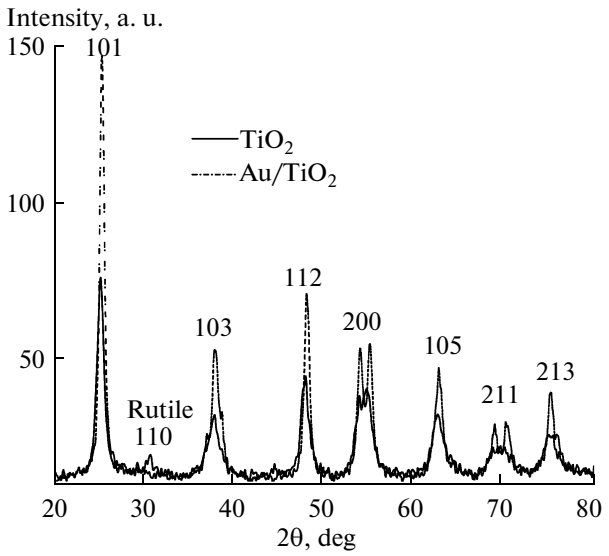

Fig. 1. XRD patterns of TiO_2 and Au/TiO_2.

After irradiation, the suspension was centrifuged and the MO, MB, RB-4 and EB content was analyzed quantitatively at 464, 660, 595 and 517.9 nm, respectively, using Cary-1E UV-vis spectrophotometer (Varian, Australia).

The GSE ANATOC-analyzer determined concentration of total organic carbon.

All the catalytic results were reproducible with ±5% variation.

RESULTS AND DISCUSSION

Characterization

Au/TiO_2 contain mostly anatase phase but in case of TiO_2 small amount of rutile phase is also present (95% anatase and 5% rutile, Fig. 1). Gold modification probably inhibits the phase transformation of TiO_2. This may be due to formation of $Au_xTi_{1-x}O_2$ type complex where some titanium ions were replaced by gold [18]. The percentage of anatase phase can be calculated by the following equation:

$$\%\ \text{of anatase phase} = \frac{100}{1 + I_R/0.79I_A},$$

where I_A and I_R are the intensity of strongest diffraction line (101) of anatase phase and (110) of rutile phase, respectively [29]. A weak peak at 44.5° in case of Au/TiO_2 may be due to the presence of less amount of gold. The reflections for polycrystalline TiO_2 planes present are {110}, {110}, {103}, {112}, {200}, {105}, {211} and {213}. Presence of these peaks is also confirmed from TEM and selected area electron diffraction (**SAED**) pattern.

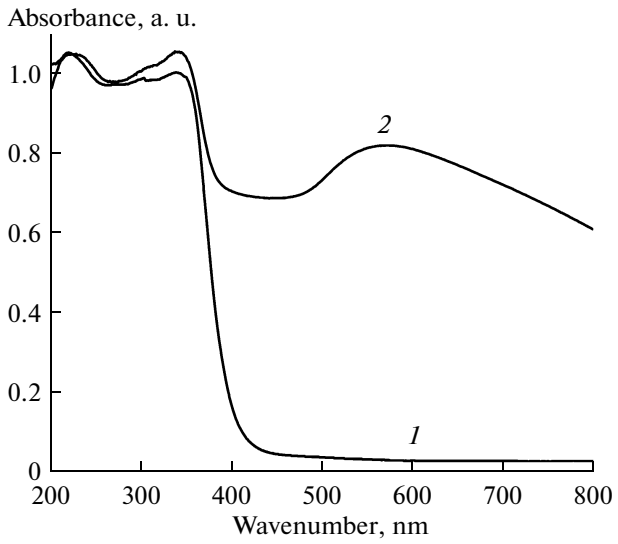

Fig. 2. UV-visible DRS spectra of TiO_2 (*1*) and Au/TiO_2 (*2*).

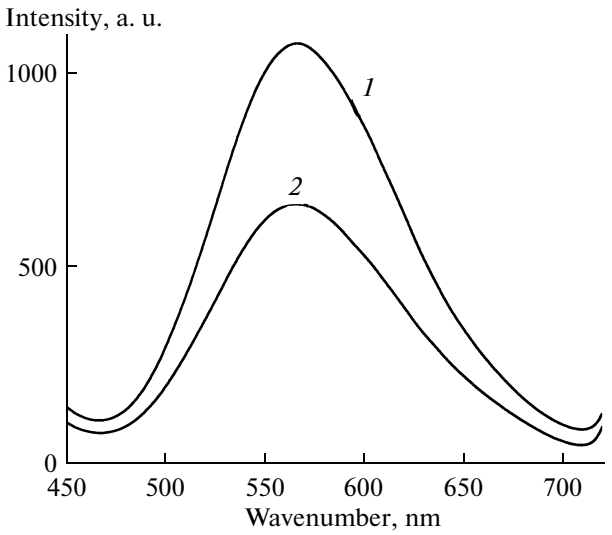

Fig. 3. Photoluminescence spectra of TiO_2 (*1*) and Au/TiO_2 (*2*) excited at 380 nm.

The crystallite sizes (D) of anatase and rutile phases were determined by employing Debye–Scherrer formula, $D = K\lambda/\beta\cos\theta$, where λ is wavelength of the CoK_α used, β is the full width at half maximum of the diffraction angle considered, K is a shape factor (0.94) and θ is the angle of diffraction. The peaks (101) for anatase and (110) for rutile were used. The crystallite size of TiO_2 (9.8 nm) is greater than Au/TiO_2 (8.8 nm). This may possibly be due to the fact that the gold modification of TiO_2 could stabilize the crystallite size.

UV-visible DRS spectra (Fig. 2) demonstrate the enhanced absorption of light in case of Au/TiO_2. The enhanced light absorption can therefore provide more photocharges needed for the photocatalytic reactions. It was found that the absorption spectrum of Au/TiO_2 was shifted toward the visible region and this might be responsible for the enhancement of photocatalytic activity under solar radiation. Significantly enhanced absorption spectra in the visible region of longer wavelength at 500–600 nm are due to the plasmon resonance of gold nanoparticles. Surface plasmon resonance of metallic gold nanoparticles depends on the particle size, shape, loading and surrounding environment. The red shift from the near UV to visible region is due to formation of $Au_xTi_{1-x}O_2$ type complex where some titanium ions were replaced by gold. The strong absorption at 200–340 nm is characteristic of the TiO_2.

To know the rate of electron/hole recombination, photoluminescence (**PL**) emission spectra was carried out. PL emission spectra of doped and un-doped TiO_2 exhibit luminescence peak at 570 nm under photoexcitation at 380 nm (Fig. 3). The physical origin of the PL may be due to the radiative recombination of self-trapped excitons localized within TiO_6 octahedra. The PL intensity of TiO_2 sample was significantly higher than that of Au/TiO_2 sample. Lower PL intensity in case of Au/TiO_2 indicates the lower recombination rate of electron/hole [18, 26]. This may be due to the fact that these excited electrons migrate to Au clusters, which capture the electrons and prevent the direct electrons and holes recombination. So, from the spectrophotometric study, the enhanced photocatalytic reaction in case of Au/TiO_2 catalyst may be due to the higher light absorption capacity, band gap shifting from near UV to visible region and lower electron/hole recombination rate, which are most essential for a good photocatalyst.

Gold nanoparticles were distributed over TiO_2 surface. From SAED pattern (Fig. 4b), the concentric diffraction rings clearly revealed the presence of {101}, {112}, {200}, and {211} plane of anatase TiO_2. This indicates highly crystalline nature of sample, which is good agreement with the XRD data. Presence of gold was confirmed by EDX spectroscopy (Fig. 3). The average particle size of gold was found to be 10.0 nm with standard deviation of ±2.6 nm. If all the dark particles (Fig. 4a) correspond to Au, it seems that their number is higher than 1 wt %. For calculating size of Au particle, we have searched such spots where more gold nanoparticles are present. But such spots are very rare. It seems 1 wt % of Au with respect to Fig. 4b. From XPS, Au content was found to be 1.3 wt %, slightly higher than the targeted value (1 wt %). The binding energy of the $Au4f_{7/2}$ was found to be 84.2 eV, indicating that gold is in metallic state.

The reduction properties of the catalysts were studied by TPR method (Fig. 6). It is well known that TiO_2

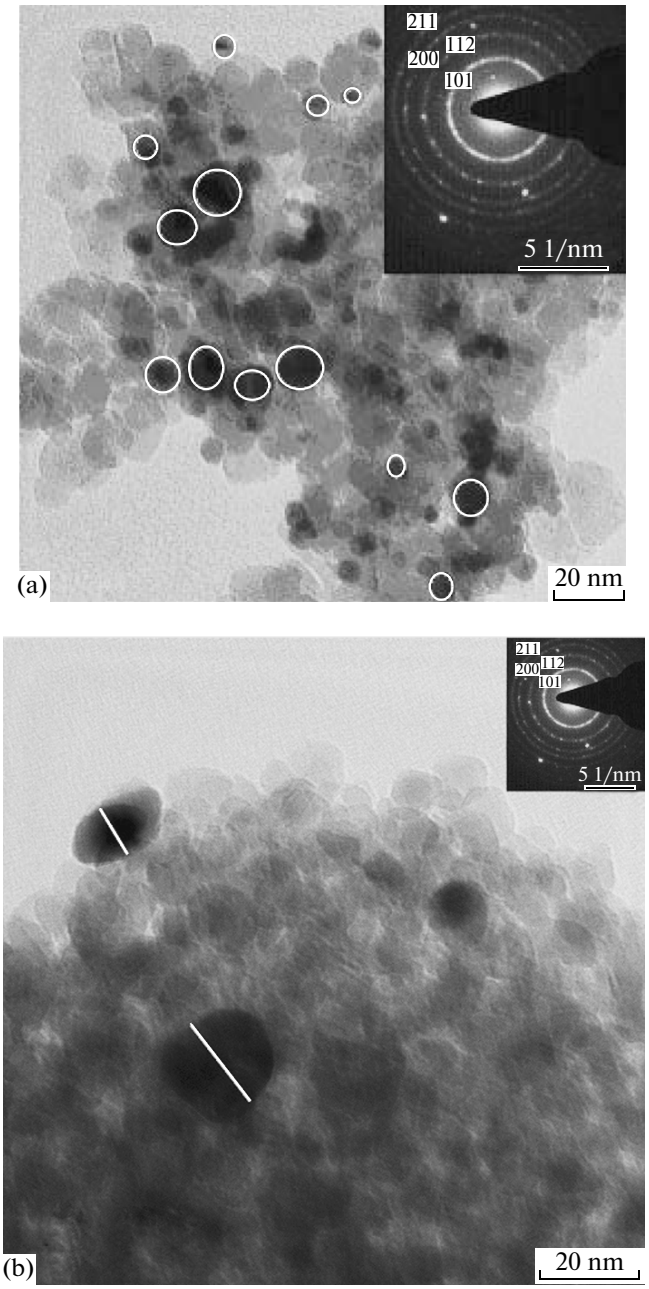

Fig. 4. TEM (a) and SAED (b) pattern of Au/TiO_2 (black particles are Au).

is reluctant to reduce even at higher temperature. But Au/TiO_2 is partially reduced to TiO_{2-x} by hydrogen at high temperatures. So the peak around 430°C is assigned to partial reduction of Ti^{4+} to Ti^{3+}. This process is promoted by the presence of dispersed metal crystallites. This may be due to the strong interaction between supports and dispersed metal oxide [30]. This interaction may be due to the charge transfer from the TiO_2 to Au nanoparticles. As large difference in the work function between Au (5.42 eV) and TiO_2 (4.7 eV) facilitated electron transfer is from TiO_2 to Au [31]. This evidence is also found from IR spectra of adsorbed CO. Adsorption of 100 mbar of CO over TiO_2 at ambient temperature exhibited an IR absorption band at 2184 cm^{-1} attributed to weakly adsorbed CO on Ti^{4+} ion (Fig. 7). Dispersion of gold on TiO_2 resulted in considerable reduction in CO adsorption on Ti^{4+} sites and appearance of this band at lower wavenumber (2180 cm^{-1}). Shifting of this band awards lower wavenumber may be due to creation of new electron-rich Au sites in the sample. Such an increase of the electron density of Au results in an increase of the

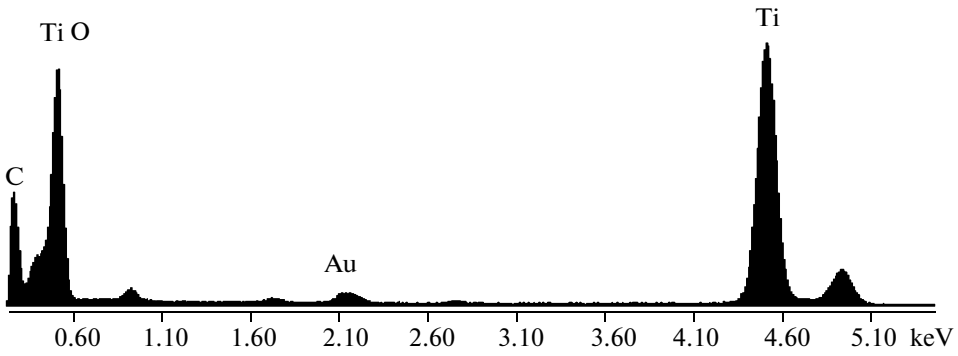

Fig. 5. Energy dispersive X-ray spectrum of Au/TiO_2.

back-donation of the metal electrons into 2p* antibonding orbitals of the CO molecule and a weakening of the C=O bond. For example, charge transfer from the oxygen vacancies on the MgO surface to the Au clusters enhanced the back donation, resulting in weakening of the C=O bond [32]. The presence of electron-rich Au sites in Au/TiO_2 suggests the existence of electronic interactions between Au and the support. The appearance of a broad band at ~2118 cm^{-1} assigned to linearly adsorbed CO on metallic gold.

Photocatalytic Activity

Degradation of dyes was found to be 5% after 4 h of irradiation in absence of catalyst. From this we can say that auto degradation of dye does not occur by absorbing visible light. In presence of Au/TiO_2 photocatalyst, 82.0% of MO and 85% of MB degradation took place under solar radiation, whereas only 15% of adsorbtion takes place under similar conditions in dark (Fig. 8).

The pH of the solution is one of the most important controlling parameter in the degradation of dyes (Fig. 9). The pH effect can be explained on the basis of point of zero charge of Au/TiO_2. Point of zero charge (**pH-pzc**) of Au/TiO_2 is 5.3–5.7. For pH lower than the pH-pzc, catalyst surface becomes positive charge, which favors the electrostatic interaction between anionic dyes like MO, RB-4, and EB. Opposite effect was found in case of pH higher than the pH-pzc. In case of MB opposite effect was found, as it is a cationic dye.

The enhancement of photocatalytic activity depends on the adsorption of substrate, optical absorption, and the electron/hole recombination. Adsorption of different dyes was found to be more in case of Au/TiO_2 as compared to TiO_2. Significantly enhanced absorption of light in the visible region was

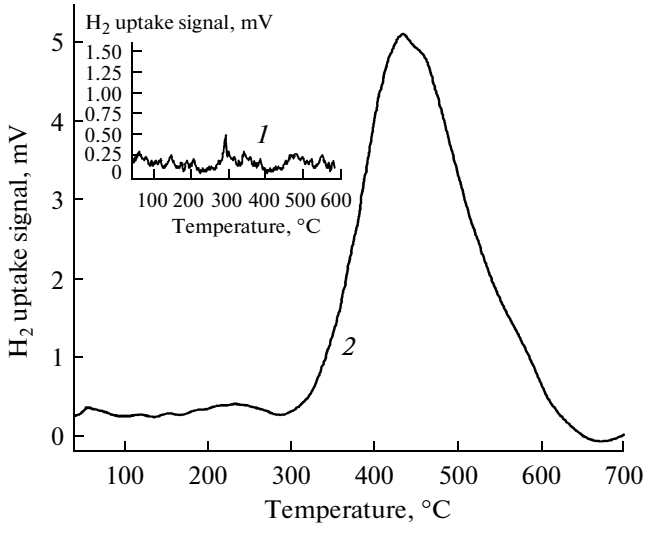

Fig. 6. Temperature-programmed reduction profiles of TiO_2 (*1*) and Au/TiO_2 (*2*).

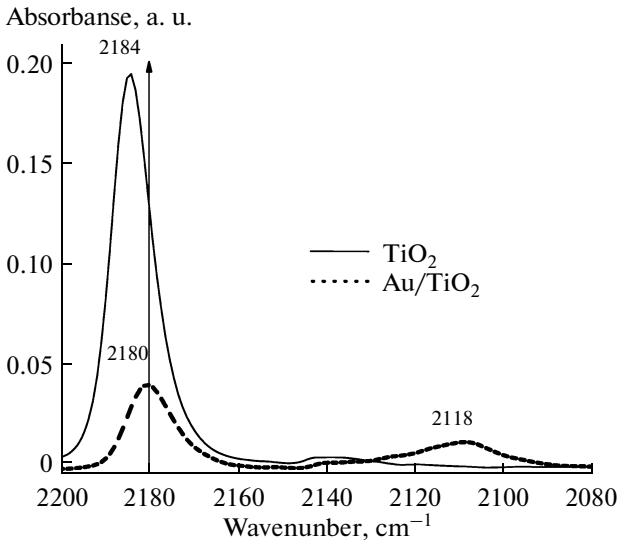

Fig. 7. IR spectra of TiO_2 and Au/TiO_2, exposure to 100 mbar CO at room temperature.

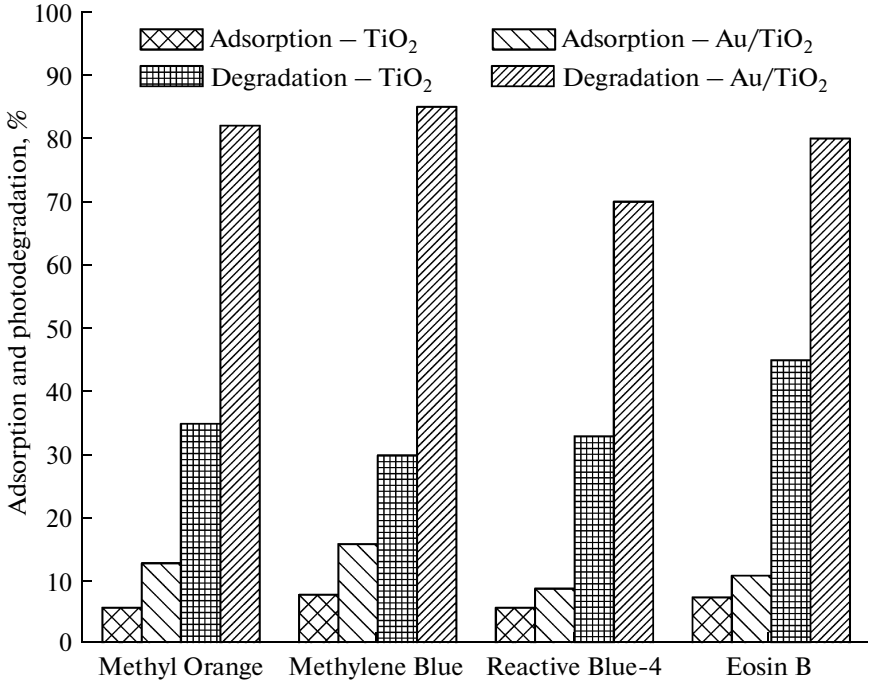

Fig. 8. Adsorption and photodegradation of dyes over TiO_2 and Au/TiO_2 under solar radiation. Catalyst concentration 1.0 g/L, dye amount 20 mL of 100 mg/L solution, time 4 h.

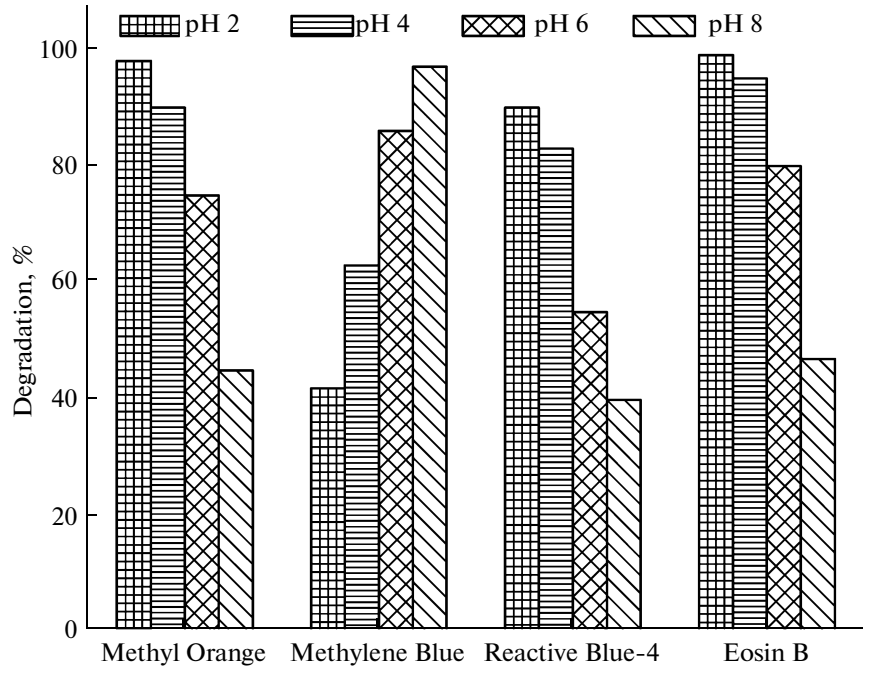

Fig. 9. Effect of pH on photocatalytic degradation of azo-dyes over Au/TiO_2 and TiO_2. Catalyst concentration 1.0 g/L, dye amount 20 mL of 100 mg/L solution, time 4 h.

found in case of Au/TiO_2, which provide more photocharges needed for the photocatalytic reactions. The Au nanoparticles in the Au/TiO_2 produce Schottky barrier, which facilitates the migration of photoexcited electron to gold. Therefore, the rate of electron/hole pairs recombination decreases, which would be beneficial to the photodegradation of organic dyes by using Au/TiO_2.

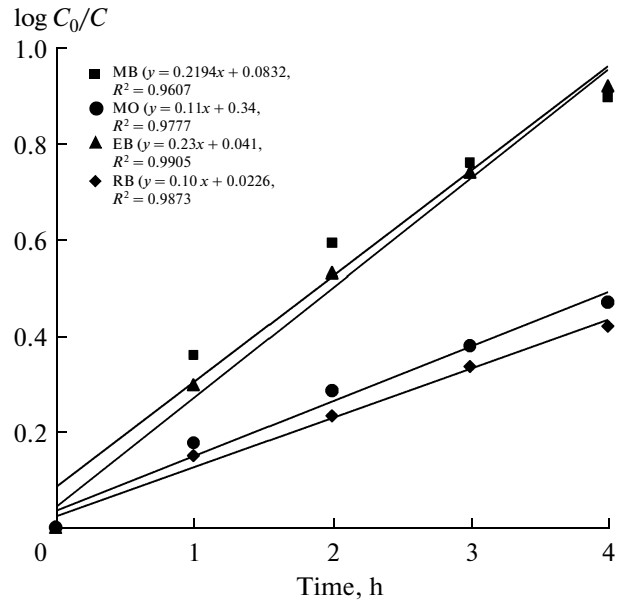

Fig. 10. Kinetics of azo-dyes degradation over Au/TiO_2. Catalyst concentration 1.0 g/L, dye amount 20 mL of 100 mg/L solution.

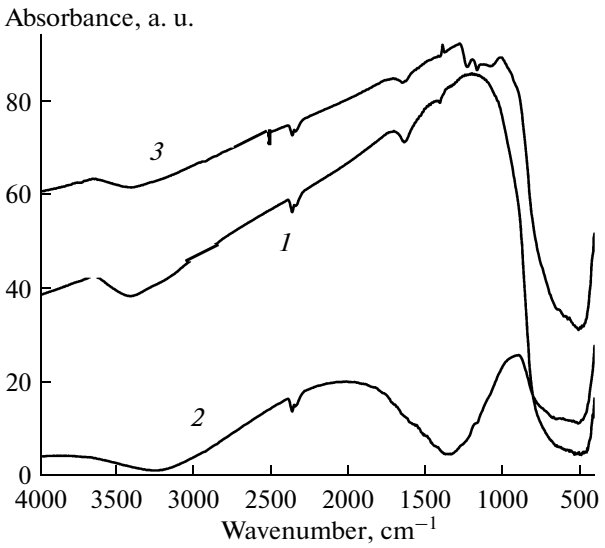

Fig. 11. Regeneration of Au/TiO_2 studied by FT-IR: *1*—fresh sample, *2*—sample after reaction, *3*—regenerated catalyst.

Kinetics of the photodegradation was studied by taking 100 mg/L dyes solutions over Au/TiO_2 and TiO_2. Photocatalytic degradation of dyes followed first order kinetics model. A linear relationship was observed between dye concentration and irradiation time as shown in Fig. 10 ($\log C_0/C$ versus time, where C_0 is the initial concentration and C is the concentration at time t). The calculated data for first order rate constants k are given in the table. The observed rate constants of TiO_2 was only one-tenth of the constant Au/TiO_2 for MB, one-third for MO, one-three and half for EB and one-fourth for RB-4 degradation. The concentrations of TOC removed were found to be 68, 78, 83.4, and 63.3% for MO, EB, MB and RB-4, respectively, over Au/TiO_2 photocatalyst after 4 h of reaction.

The catalyst was tested in recycling experiments. After prolonged reaction, slight decrease in photocatalytic activity is due to the presence of adsorbed MB. After three cycles of reaction, catalytic activity of Au/TiO_2 was decreased by 10%. In order to regenerate the catalyst, it was separated by filtration, washed several times with distilled water and dried at 110°C. The material calcined at 300°C was used in the fresh reaction mixture. From FT-IR spectrum of regenerated sample (Fig. 11) it was found that activation at 300°C leads to complete removal of adsorbed MB, leaving the catalyst to its original form. The IR spectrum of the Au/TiO_2 sample after reactions (uncalcined) has highly intense peak at 1385 cm^{-1}. In case of uncalcined sample a broad peak at 1385 cm^{-1} was assigned

Kinetics parameters of the photodegradation

Dye	Au/TiO_2		TiO_2	
	k, h^{-1}	correlation coefficient R^2	k, h^{-1}	correlation coefficient R^2
MB	0.573	0.961	0.055	0.992
MO	0.324	0.978	0.126	0.973
EB	0.604	0.995	0.171	0.981
RB-4	0.278	0.987	0.066	0.964

Note. 20 mL of 100 mg/L dyes solution, 1 g/L of Au/TiO_2 and TiO_2, time of photodegradation 1, 2, 3 and 4 h.

to symmetric stretching of C–N bond presented in MB, which disappeared after calcination at 300°C.

So, higher photocatalytic activity of Au/TiO_2 compared to TiO_2 can be explained by considering the following aspects: enhanced light absorption, shifting of absorption from UV to visible spectral region and reduction in electron/hole recombination. Au/TiO_2 was found to be highly crystalline and there a strong metal–support interaction exists. The catalyst can be regenerated many times without appreciable loss in catalytic activity. Photocatalytic degradation of azo-dyes is pH dependent. Degradation rate follows first order kinetics model.

Authors are greatly acknowledged Prof. B.K. Mishra, Director, IMMT, Bhubaneswar for support and permission and BRNS for financial support.

REFERENCES

1. Schiavello, M., *Photocatalysis and Environment*, Dordrecht: Kluwer, 1998.
2. *Photocatalytic Purification and Treatment of Water and Air*, Ollis, D.F. and Al-Ekabi, H., Eds., Amsterdam: Elsevier, 1993.
3. Kamat, P.V., *Chem. Rev.*, 1993, vol. 93, p. 267.
4. Hoffmann, M.R., Martin, S.T., Choi, W., and Bahnemann, D.W., *Chem. Rev.*, 1995, vol. 95, p. 69.
5. Lachheb, H., Puzenat, E., Houas, A., Ksibi, M., Elaloui, E., Guillard, C., and Herrmann, J.-M., *Appl. Catal., B*, 2002, vol. 39, p. 75.
6. Hadjiivanov, K.I. and Klissurski, D.G., *Chem. Soc. Rev.*, 1996, vol. 25, p. 61.
7. Stylidi, M., Kondarides, D., and Verykios, X.E., *Appl. Catal., B*, 2003, vol. 40, p. 271.
8. Murakami, N., Fujisawa, Y., Tsubota, T., and Ohno, T., *Appl. Catal., B*, 2009, vol. 92, p. 56.
9. Choi, W., Termin, A., and Hoffmann, M., *J. Phys. Chem.*, 1994, vol. 98, p. 13669.
10. Zhang, A., Zhang, R.B., Zhang, N., Hong, S.G., and Zhang, M., *Kinet. Catal.,* 2010, vol. 51, p. 529.
11. Zhang, A., Zhang, S.G., Hong, S.G., and Zhang, M., *Kinet. Catal.*, 2009, vol. 50, p. 748.
12. Shi, J., Zheng, J., Hu, Y., and Zhao, Y., *Kinet. Catal.*, 2008, vol. 49, p. 279.
13. Haruta, M., Yamada, N., Kaboyashi, T., and Iijima, S., *J. Catal.*, 1989, vol. 115, p. 301.
14. Bond, G.C. and Thompson, D.T., *Gold Bull.*, 2000, vol. 33, p. 41.
15. Chen, M.S. and Goodman, D.W., *Science*, 2004, vol. 306, p. 252.
16. Kamat, P.V., *J. Phys. Chem. B*, 2000, vol. 104, p. 10851.
17. Subramanian, V., Wolf, E., and Kamat, P.V., *J. Phys. Chem. B*, 2001, vol. 105, p. 11439.
18. Li, X.Z. and Li, F.B., *Environ. Sci. Technol.*, 2001, vol. 35, p. 2381.
19. Arabatzis, I., Stergiopoulos, T., Andreeva, D., Kitova, S., Neophytides, S., and Falaras, P., *J. Catal.*, 2003, vol. 220, p. 127.
20. Iliev, V., Tomova, D., Todorovska, R., Oliver, D., Petrov, L., Todorovsky, D., and Uzunova-Bujnova, M., *Appl. Catal., A*, 2006, vol. 313, p. 115.
21. Sonawane, R.S. and Dongare, M.K., *J. Mol. Catal. A: Chem.*, 2006, vol. 243, p. 68.
22. Li, H., Bian, Z., Zhu, J., Huo, Y., Li, H., and Lu, Y., *J. Am. Chem. Soc.*, 2007, vol. 129, p. 4538.
23. Ismail, A., Bahnemann, D., Bannat, I., and Wark, M., *J. Phys. Chem. C,* 2009, vol. 113, p. 7429.
24. Wang, X., Mitchell, D.R., Prince, K., Atanacio, A.J., and Caruso, R.A., *Chem. Mater.*, 2008, vol. 20, p. 3917.
25. Jung, J., Wang, M., Kim, E., Park, C., and Hahn, S., *Appl. Catal., B*, 2008, vol. 84, p. 389.
26. Yu, J., Yue, L., Liu, S., Huang, B., and Zhang, X., *J. Colloid Interface Sci.*, 2009, vol. 334, p. 58.
27. Singh, B.P., Jena, J., Besra, L., and Bhattacharjee, S., *J. Nanopart. Res.*, 2007, vol. 9, p. 797.
28. Parida, K.M., Sahu, N., Tripathi, A.K., and Kamble, V.S., *Environ. Sci. Technol.*, 2010, vol. 44, p. 4155.
29. Yan, X., He, J., Evans, D., Duan, X., and Zhu, Y., *Appl. Catal., B*, 2005, vol. 55, p. 243.
30. Haller, G.L. and Resasco, D.E., *Adv. Catal.*, 1989, vol. 36, p. 173.
31. Ioannides, T. and Verykios, X.E., *J. Catal.*, 1996, vol. 161, p. 560.
32. Yoon, B., Hakkinen, H., Landman, U., Worz, A., Antonietti, J., Abbet, S., Judai, K., and Heiz, U., *Science,* 2005, vol. 307, p. 403.